Power Losses Aware Nonlinear Model Predictive Control Design for Active Cell Balancing

Ali Arshad Uppal[1], Syed Bilal Javed [2] and Qadeer Ahmed[3]

***Abstract*—Active cell balancing guarantees good performance and long life of a battery pack. In this paper a high-fidelity model, considering the static and dynamic parameters, is developed for computing the balancing currents and power losses of an active cell balancing network (ACBN). The model comprises any two adjacent Li-ion cells connected in series and a bidirectional buck-boost converter. This model is employed to design a nonlinear model predictive controller (NMPC), which minimizes the balancing speed and power losses of ACBN. The stability of the closed-loop system is proved using Lyapunov method. The cells' state of charge (SoC) levels required for NMPC are estimated by a state dependent Kalman filter (SDKF). The control scheme is solved using CasADi toolbox, employing the interior point optimizer (Ipopt) algorithm. Despite the modeling mismatch, sensor noises, and an urban dynamometer driving schedule (UDDS) input current profile, the SoC difference stays in a legitimate range of 2%. Moreover, it has been shown that for the same controller, there is a 78.6% deviation in the balancing time if static and dynamic model parameters (e.g. charging and discharging path resistances, time delays, and time constants) are ignored.**

***Index Terms*—Active cell balancing, nonlinear model predictive control, bidirectional buck-boost converter.**

I. Introduction

The battery pack of electric vehicles (EVs) is comprised of series and parallel strings of cells to meet different current and voltage demands. The issue of cell-to-cell imbalance arises in series connected cells, which results in slower but persistent degradation of the battery pack [1]. This issue is mitigated by cell equalization methods, which are broadly categorized as passive and active cell balancing methods. The former is a dissipative method, while the latter is non-dissipative and transfers the excess charge of one cell to other cell/s or battery pack [2]. Active cell balancing methods have high balancing efficiency and are implemented using power electronics circuits, such as switching capacitor networks, buck-boost and flyback converters, etc, [3], [4].

According to the literature, cell balancing based on state of charge (SoC) equalization is preferred over terminal voltage based equalization methods [5]. The focus of this paper is the model-based optimal control of an active cell balancing network (ACBN). In literature the task of SoC equalization has been taken up to achieve various objectives pertaining to EVs and other applications. In [6] cell-to-cell balancing is performed using a bidirectional Cuk converter. The optimization problem is solved using sequential quadratic programming algorithm, which minimizes the balancing currents, and the difference in SOC of cells with average SoC of cells in the pack. The results are improved in [7] by incorporating temperature dynamics. In [8], the authors employ active cell balancing to solve range maximization problem for EVs using reachability analysis. The solution is further improved by using nonlinear model predictive control (NMPC) in [1], [9]. Liu et al. [5] solve a multi-objective optimal control problem–minimizing the balancing speed and power losses in an ACBN, by employing NMPC, which exploits differential flatness to solve pseudo spectral optimization problem. In [10] an adaptive MPC is designed to mitigate the differences in the terminal voltages of cells, which are estimated by recursive least square method. Quan et al. [11] solve the optimal control problem similar to [6] using conjugate gradient method. In [4] cell balancing is employed to extend range of an EV by formulating and solving three NMPC problems: all cells follow the nominal cell trajectory, maximization of SoC/voltage of the lowest cell and minimizing the difference between highest and lowest SoC/voltage of cells. In [12], a convex optimization problem is formulated to balance the SoC of cells by simultaneously addressing single cell equalization, thermal balancing and terminal voltage equalization problems.

In recent years, physics informed electro-chemical models of a cell are also exploited for nonlinear optimal control of active cell balancing. In [2], a single particle model with electrolyte and temperature (SPMeT) dynamics is utilized to formulate an NMPC problem, which minimizes various conflicting costs. Vahid Azimi et al. [13] employ an SPM model with aging and thermal dynamics to formulate and solve a nonlinear optimal control problem for fast charging-minimum degradation of an LiB.

Efforts have been made to include more accurate cell models, however, detailed modeling of the network is often ignored. It has been discussed in [3], that the performance of ACBN is greatly influenced by static and dynamic parameters. In this paper, high fidelity mathematical models are derived for balancing currents and power losses of the ACBN, which takes into account the effect of static and dynamic parameters as shown in Section II. In the best of the authors' knowledge such detail modeling is often ignored in the paradigm of ACBN control. The ACBN is comprised of bi-directional buck-boost converter and a battery pack with any two adjacent Li-ion cells connected in series. A first order nonlinear equivalent circuit model (ECM) represents the dynamics of a cell. The model is then employed to design an NMPC, which computes the required duty cycles (for two switches) of the buck-boost

[1] A. A. Uppal is with COMSATS University Islamabad, Islamabad, Pakistan, ali_arshad@comsats.edu.pk

[2] S. B. Javed is with Centers of Excellence in Science & Applied Technologies, s.bilal.javed@gmail.com

[3]Q. Ahmed is with The Ohio State University, ahmed.358@osu.edu

converter to equalize the SoC levels of cells. The stability of the closed-loop system is also proved using Lyapunov theory. The SoC levels required to design NMPC are estimated using a state dependent Kalman filter (SDKF). In order to test the robustness of the control technique practical considerations like parametric variations, sensor noises, and an urban dynamometer driving schedule (UDDS) input current profile are also incorporated in the simulation study. The evaluation results show that the controller keeps the SoC difference of the cells within a prescribed limit of 2%.

The rest of the paper is organized in the following manner. The mathematical modeling of the ACBN is presented in section II, which is followed by NMPC and SDKF designs in sections III and IV, respectively, and the paper is concluded in section VI.

II. Mathematical Modeling of Active Cell Balancing Network

The active cell balancing of two series connected cells is performed using bidirectional buck-boost converter, operated in discontinuous current mode, as shown in figure 1, which also shows a detailed interaction of an EV with ACBN. When cell-1 has higher SoC, the MOSFET Q_1 is turned on and the excess charge is transferred to inductor L, which is then used to charge cell-2 through diode D_2 (parallel to Q_2). Similarly, excess charge in cell-2 is transferred to cell-1 through Q_2 and D_1 (parallel to Q_1). It is important to mention that Q_1 and Q_2 can not be turned on simultaneously.

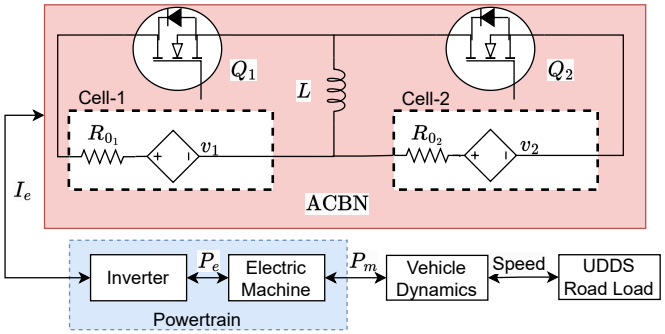

Fig. 1: Interaction of electric vehicle with ACBN (I_e is UDDS current, and P_m and P_e are mechanical and electrical powers, respectively).

A. Mean Balancing Currents in ACBN

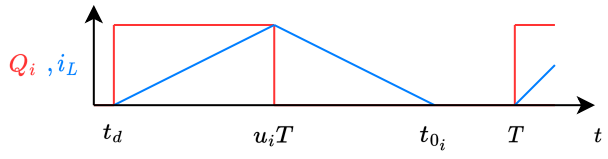

Fig. 2: Switching cycle of Q_i and mean balancing current.

The switching period of Q_i and the corresponding inductor current i_L is shown in figure 2, which is expressed as

$$i_L = \begin{cases} 0, & 0 \le t \le t_d \\ \dfrac{v_H}{R_{ch_i}}\left(1-\exp\left(\lambda_i\right)\right), & t_d \le t \le u_iT \\ \exp\left(\phi_i\right)\left(I_{P_i}+\dfrac{v_L+V_F}{R_{dis_i}}\right)-\dfrac{v_L+V_F}{R_{dis_i}}, & u_iT \le t \le t_{0_i} \\ 0, & t_{0_i} \le t \le T \end{cases}, \tag{1}$$

$$\lambda_i = \frac{t_d - t}{\tau_{ch_i}},\ \phi_i = \frac{u_iT - t}{\tau_{dis_i}},\ R_{dis_i} = R_{0_L} + R_L,$$
$$R_{ch_i} = R_{0_H} + R_L + R_{ds},\ \tau_{ch_i} = L/R_{ch_i},\ \tau_{dis_i} = L/R_{dis_i},$$

where $i = 1$ and $i = 2$ represent cell-1 charging cell-2 and cell-2 charging cell-1, respectively; v_H, v_L and R_{0_H}, R_{0_L} represent open circuit voltages (V) and resistances (Ω) of higher and lower SoC cells, respectively; V_F is diode forward voltage drop, τ_{ch} and τ_{dis} are time constants (s) for charging and discharging paths, respectively; t_d, t_0 and T represent dead time, time instant at which $i_L = 0$, and switching time period, respectively; duty cycle of Q_i is denoted by u_i, and L represents the inductance of the inductor (H); and R_{ch}, R_{dis}, R_L and R_{ds} represent resistances of charging path, discharging path, cell i, inductor and on-state switching, respectively.

When charge is transferred from cell-1 to cell-2 then $u_i = u_1$, $v_H = v_1$ and $v_L = v_2$, whereas, $u_i = u_2$, $v_H = v_2$ and $v_L = v_1$ when cell-2 charges cell-1.

Equation (1) can be integrated over the complete switching period to yield mean currents for charging and discharging modes of inductor

$$\tilde{I}_{ch_i} = \frac{v_H}{TR_{ch_i}}\left(u_iT - t_d + \tau_{ch_i}\left(\exp\left(\kappa_i\right)-1\right)\right), \tag{2}$$

$$\tilde{I}_{dis_i} = \frac{\tau_{dis_i}\left(\exp\left(\chi_i\right)-1\right)}{T}\left(-I_{P_i} - \frac{a_{0_i}(t_{0_i}-u_iT)}{\tau_{dis_i}\left(\exp\left(\chi_i\right)-1\right)} + 1\right), \tag{3}$$

$$I_{P_i} = \frac{v_H}{R_{ch_i}}\left(1-\exp\left(\kappa_i\right)\right),\ \kappa_i = \frac{t_d - u_iT}{\tau_{ch_i}},$$
$$t_{0_i} = u_iT + \tau_{dis_i} ln\left(\frac{R_{dis_i}v_H}{(v_L+V_F)R_{ch_i}}\left(1-\exp\left(\kappa_i\right)\right)+1\right),$$
$$\chi_i = \frac{u_iT - t_{0_i}}{\tau_{dis_i}},\ a_{0_i} = \frac{v_L+V_F}{R_{dis_i}},$$

where $\tilde{I}_{ch}$ and $\tilde{I}_{dis}$ are mean currents (A) during charging and discharging modes of inductor, respectively, and I_p is the peak inductor current at $t = u_iT$ (cf. figure 2).

B. Power Losses in the Buck-Boost Converter

The total power losses in the ACBN are sum of the following losses:

1) Conduction Power Losses: The power losses due to on-state resistances of MOSFETs, diodes, parasitic resistances

of energy storage elements and internal resistances of cells constitute the conduction losses, which are characterized as

$$P_{con_i} = I^2_{ch_i} R_{ch_i} u_i + I^2_{dis_i} R_{dis_i} \left(\frac{t_{0_i} - u_i T}{T} \right) + I^2_{b_i} R_{0_i},$$

$$I^2_{ch_i} = \frac{v^2_H}{T R^2_{ch_i}} \left[\tau_{ch_i} \exp(\kappa_i) \left(\frac{4 - \exp(\kappa_i)}{2} \right) \right] + \frac{v^2_H}{T R^2_{ch_i}} \left[u_i T - t_d - \frac{3}{2} \tau_{ch_i} \right],$$

$$I^2_{dis_i} = \frac{1}{T} \left[\tau_{dis_i} I_{P_i} \left(\frac{I_{P_i}}{2} - a_{0_i} \right) + a^2_{0_i} \left(t_{0_i} - u_i T - \frac{3}{2} \tau_{dis_i} \right) \right] + \frac{1}{T} \left[-\tau_{dis_i} \exp(2\kappa_i) \left(\frac{I^2_{P_i}}{2} + \frac{a^2_{0_i}}{2} + a_{0_i} I_{P_i} \right) \right] + \frac{1}{T} \left[\exp(3\kappa_i) 2 a_{0_i} \tau_{dis} \left(I_{P_i} + a_{0_i} \right) \right], \quad (4)$$

where I_{b_i}, cf. (10), (11), is the current of cell-i, $P_{con} = P_{con_1} + P_{con_2}$ are conduction losses (W), and I_{ch} and I_{dis} represent the effective RMS currents during charging and discharging modes, respectively.

2) Switching Power Losses: As the buck-boost converter is operated in discontinuous conduction mode, therefore, the switching losses ($P_{t_f} = P_{t_{f_1}} + P_{t_{f_2}}$) only consider the power losses when MOSFETs are turned off

$$P_{t_{f_i}} = \frac{1}{2T} v_H \tilde{I}_{dis_i} t_f, \quad (5)$$

where t_f is the fall time.

3) Reverse Recovery Power Losses in Body Diode: The reverse recovery power loss associated with the body diode D_i is

$$P_{D_{rr_i}} = \frac{1}{2T} v_L I_{rr_i} t_{rr}, \quad (6)$$
$$I_{rr_i} = \sqrt{2 Q_{rr_i} \left(\frac{v_L + V_F}{L} \right)},$$
$$Q_{rr_i} = t^2_{rr} \left(\frac{v_L + V_F}{2L} \right),$$

where $P_{D_{rr}} = P_{D_{rr_1}} + P_{D_{rr_2}}$, Q_{rr}, I_{rr} and t_{rr} denote the reverse recovery power loss, charge, current and time, respectively.

4) Dead Time Power Losses: During dead time both Q_1 and Q_2 are off and the inductor current keeps on flowing through the body diodes

$$P_{t_{d_i}} = \frac{1}{2T} V_F \tilde{I}_{dis_i} t_d, \quad (7)$$

where $P_{t_d} = P_{t_{d_1}} + P_{t_{d_2}}$ represents dead time power loss and t_d represents the dead time.

C. Equivalent Circuit Model of the Battery Pack

The battery pack has two series connected cells as shown in figure 1. A simple ECM of a cell is selected which is comprised of the internal resistance R_{0_i} in series with a dependent voltage source representing the open circuit voltage v_i. The control-oriented model of the battery pack is given as

$$\dot{\vec{x}} = \vec{f}(\vec{x}, \vec{u}) = \begin{bmatrix} \frac{I_{b_1}}{\eta_1} & \frac{I_{b_2}}{\eta_2} \end{bmatrix}^T, \quad (8)$$

$$\vec{v}_t = \vec{h}(\vec{x}, \vec{u}) = \begin{bmatrix} v_1 + I_{b_1} R_{0_1} & v_2 + I_{b_2} R_{0_2} \end{bmatrix}^T, \quad (9)$$

$$I_{b_1} = -\tilde{I}_{ch_1}(u_1, x_1) + \tilde{I}_{dis_2}(u_2, x_1, x_2) + I_e(t), \quad (10)$$

$$I_{b_2} = -\tilde{I}_{ch_2}(u_2, x_2) + \tilde{I}_{dis_1}(u_1, x_1, x_2) + I_e(t), \quad (11)$$

$$v_i = \sum_{j=1}^{8} p_j x_i^{(8-j)}, \quad (12)$$

where $\vec{x} \in \Re^2$ is the state vector representing SoC of cell-1 (x_1) and cell-2 (x_2), respectively; $\vec{u} \in \Re^2$ is the control vector, which represents duty cycle of Q_1 and Q_2, respectively; $\vec{v}_t \in \Re^2$ represents the terminal voltages of the cells; η_i is capacity of cell-i (As); and $p = [88.56, -320.46, 472.36, -368.96, 166.57, -44.01, 7.18, 2.95]$.

III. Nonlinear Model Predictive Control of Active Cell Balancing

The objective of the cell balancing controller is to minimize $|\tilde{x}| = |x_1 - x_2|$. As the control problem has to be solved in the presence of multiple constraints on state and control variables, therefore, we propose the following NMPC problem.

Let $\{t_i\}_{i \geq 0}$, such that $t_{i+1} = t_i + \delta$, where $\delta > 0$ is the sampling time. Now, the implementation of NMPC is carried out in the following manner. The current SoC difference $\tilde{x}(t_i)$ is obtained, then the following nonlinear optimal control problem (NOCP) is solved to obtain optimal control ($\bar{\vec{\mu}}$) and state ($\bar{\vec{x}}$) trajectories

$$\begin{aligned} &\min_{\vec{x}, \vec{\mu}} \int_{t_i}^{t_i + T_p} \left(Q \tilde{x}^2 + R P_L^2 \right) d\mathcal{T}, \\ &subject\ to \\ &\dot{\vec{x}} - \vec{\tilde{f}}(\vec{x}, \vec{\mu}) = 0, \quad a.e.\ t \in [t_i, t_i + T_p], \\ &\vec{x}(t_i) = \vec{x}_{t_i}, \\ &\vec{\mu} \in [\vec{\mu}_{lb},\ \vec{\mu}_{ub}] \quad a.e.\ t \in [t_i, t_i + T_p], \\ &\vec{x}(t) \in [\vec{x}_{lb},\ \vec{x}_{ub}], \quad a.e.\ t \in [t_i, t_i + T_p], \\ &\mu_1 \mu_2 = 0, \quad a.e.\ t \in [t_i, t_i + T_p], \end{aligned} \quad (13)$$

where $\vec{\mu} = \vec{u} - t_d/T$, such that $\vec{\tilde{f}}(0, 0) = 0$; T_p is the prediction horizon (s); $P_L = P_{con} + P_{tf} + P_{D_{rr}} + P_{t_d}$ represents total power losses; $Q > 0$, $R > 0$ are scalar weights: $\vec{\mu}_{lb}$, $\vec{\mu}_{ub}$, $\vec{x}_{lb}$ and $\vec{x}_{ub}$ are lower and upper bounds on input $\vec{\mu}$ and state vector $\vec{x}(t)$, respectively.

The closed loop input for interval $[t_i, t_i + \delta]$ is $\vec{\mu}^* := \bar{\vec{\mu}}(t_i)$, whereas, the remaining elements of $\bar{\vec{\mu}}$ are discarded. The procedure is repeated for every sampling instant to solve the NMPC problem.

The nominal stability of NMPC can be established by proving that the cost functional in (13) decreases with time and

eventually vanishes. Let us consider the following candidate Lyapunov functional

$$V(\tilde{x},\vec{\mu}) = Q\tilde{x}^2 + RP_L^2 \leq Q\tilde{x}^2 + Rw^2, \tag{14}$$

where $V(\tilde{x},\vec{\mu})$ is strictly positive definite.

The last constraint in (13) ensures that both Q_1 and Q_2 can not be turned on simultaneously, therefore, $w = \mu_1$–cell-1 charging cell-2 or $w = \mu_2$–cell-2 charging cell-1. Furthermore, from the nominal mathematical model of the ACBN it can be easily shown that $|w| > |P_L|$. By substituting $w = -Kx$ ($K \in \Re$ is the state feedback gain) in (14) and taking its time derivative yields

$$\dot{V}(\tilde{x},K\tilde{x}) \leq 2Q\tilde{x}\dot{\tilde{x}} + 2RK^2\tilde{x}\dot{\tilde{x}} = -\Gamma|\tilde{x}\dot{\tilde{x}}|, \tag{15}$$

where $\Gamma = 2Q + 2RK^2 > 0$, and from (8) it can be seen that $\tilde{x}\dot{\tilde{x}} < 0$, because the currents $\tilde{I}_{ch}$ and $\tilde{I}_{dis}$ in (2) and (3) are positive. Therefore, $\dot{V}(\tilde{x},K\tilde{x})$ is negative definite and the nominal closed-loop system is stable.

The SoC levels of cells required for NMPC design are estimated using a state dependent Kalman filter (SDKF).

IV. State Dependent Kalman Filter

The design of SDKF is comprised of three steps: (i) representing the nonlinear model in (8) and (9) by state dependent matrix form, cf. [14]; (ii) discretising the quasi-linear ECM model and (iii) employing the conventional Kalman filter algorithm to estimate x_1 and x_2. For observer design I_{b_i} and v_t in (8) and (9) are measurable, therefore, the ECM for the battery pack can be re-written as

$$\dot{\vec{x}} = B\vec{I} + \vec{\psi}(t), \tag{16}$$

$$\vec{y} = \begin{bmatrix} v_{t_1} - p_8 \\ v_{t_2} - p_8 \end{bmatrix} = C(\vec{x})\vec{x} + D\vec{I} + \vec{\phi}(t), \tag{17}$$

where $\vec{\psi}(t)$ is the process noise, $\vec{\phi}(t)$ represents the measurement noise, $\vec{I} = [I_{b_1} \quad I_{b_2}]^T$, and $p_8 = 2.95$. The matrices B, $C(\vec{x})$ and $D(\vec{x})$ are expressed as

$$B = diag\left(\eta_1^{-1}, \eta_2^{-1}\right),\ D = diag\left(R_{0_1}, R_{0_2}\right)$$

$$C(\vec{x}) = \begin{cases} diag\Big(c_1(x_1), c_2(x_2)\Big), & \vec{x} \neq 0, \\ diag\Big(\nabla h_1(x_1), \nabla h_2(x_2)\Big), & \vec{x} = 0, \end{cases}$$

$$c_i(x_i) = \nabla h_i(x_i) + \left(\frac{h_i(x_i) - x_i^T \nabla h_i(x_i)}{x_i^T x_i}\right) x_i,$$

$$\nabla h_i(x_i) = \sum_{j=1}^{7} (8-j) p_j x_i^{7-j}, \tag{18}$$

where $\nabla h_i(x_i)$ is the gradient of h_i with respect to x_i. It is pertinent to mention here that quasi-linearization is only performed for (12), which results in state dependent matrix $C(\vec{x})$.

After performing the quasi-linear decomposition, the system given in (16) and (17) is discretised with the sampling time δ (same as in MPC design) to yield the following structure of the SDKF (which is implemented according to algorithm 1)

$$\vec{x}_k = G_{k-1}\vec{I}_{k-1} + \vec{\psi}_{k-1},$$
$$\vec{y}_k = C_k\vec{x}_k + D_k\vec{I}_k + \vec{\phi}_k, \tag{19}$$

where $G = B(\vec{x})\delta$, and $\vec{\psi}_k$ and $\vec{\phi}_k$ are white, zero-mean, uncorrelated noise processes with known covariance matrices $\mathcal{Q}_k$ and $\mathcal{R}_k$, respectively, which are characterized as

$$\vec{\psi}_k \sim (0, \mathcal{Q}_k),\ \vec{\phi}_k \sim (0, \mathcal{R}_k),\ E\left[\vec{\psi}_k\vec{\psi}_j^T\right] = \mathcal{Q}_k\delta_{k-j},$$
$$E\left[\vec{\phi}_k\vec{\phi}_j^T\right] = \mathcal{R}_k\delta_{k-j},\ E\left[\vec{\phi}_k\vec{\psi}_j^T\right] = 0,$$

where the Kronecker delta function $\delta_{k-j} = 1$ if $k = j$ and $\delta_{k-j} = 0$ if $k \neq j$.

Algorithm 1 SDKF Algorithm

1: **Initialization:** the state vector $\left(\vec{\hat{x}}\right)$ and estimation error covariance matrix ($P \in \Re^{2\times 2}$) are initialized as

$$\vec{\hat{x}}_0^+ = E\left(\vec{x}_0\right),$$
$$P_0^+ = E\left[\left(\vec{x}_0 - \vec{\hat{x}}_0^+\right)\left(\vec{x}_0 - \vec{\hat{x}}_0^+\right)^T\right],$$

where the superscript $^+$ denotes a posteriori estimate, which takes into account all the measurements up to time k.

2: **while** $1 \leq k \leq k_{end}$ **do**

3: **Prediction:** the a-priori estimates (which does not consider current measurement) of SDKF gain K_k^-, P_k^- and $\hat{x}_k^-$ are computed as

$$P_k^- = \mathcal{Q}_{k-1},$$
$$K_k^- = P_k^- C_k^T \left(C_k P_k^- C_k^T + \mathcal{R}_k\right)^{-1},$$
$$\vec{\hat{x}}_k^- = G\vec{\hat{I}}_{k-1}.$$

4: **Correction:** by using the current measurement the estimated state and error covariance matrix are updated as

$$\vec{\hat{x}}_k^+ = \vec{\hat{x}}_k^- + K_k\left[\vec{y}_k - \left(C_k\vec{\hat{x}}_k^- + D_k\vec{\hat{I}}\right)\right],$$
$$P_k^+ = \left(I_2 - K_kC_k\right)P_k^-\left(I_2 - K_kC_k\right)^T + K_k\mathcal{R}_kK_k^T.$$

5: $k = k + 1$

6: **end while**

V. Results and Discussions

The implementation scheme considered for the simulation studies is presented in figure 3. Based on the measurements of $\vec{v_t}$ and $\vec{I}$, SDKF reconstructs SoC levels of cells, which are further utilized by NMPC to compute the duty cycle for the buck-boost converter. The problem of active cell balancing is solved in Matlab/Simulink. The nominal values of LG 18650HG2 cell (cf. [15]) and other ACBN parameters are given in table I.

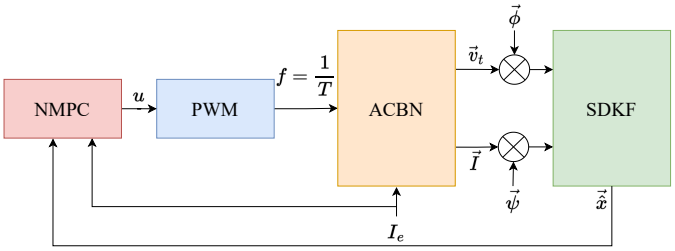

Fig. 3: Control architecture for active cell balancing.

TABLE I: Nominal model parameters of ACBN

Parameter	Value	Parameter	Value
T	20 μs	t_d	2 μs
V_F	0.3 V	R_{ds}	5.3 mΩ
t_f	8 ns	t_{rr}	28 ns
R_L	0.01 Ω	L	6 μH
R_{0_i}	0.025 Ω	η_i	10800 As

The practical considerations to asses the robustness of the control scheme are: i) $R_{0_i} = 0.03\Omega$ and $\eta_i = 9000$As are used in the ACBN, whereas, nominal parameters are used in SDKF and NMPC; ii) the noises for voltage and current sensors are $\phi_i \sim \mathcal{N}(0, 10^{-4})$ and $\psi_i \sim \mathcal{N}(0, 0.01)$, respectively; iii) a UDDS current profile (I_e), cf. [16] is provided to ACBN. Moreover, the step size for performing simulations is $\delta = 5$ s. These are the default simulation parameters unless otherwise stated.

The NOCP in (13) is solved using CasADi [17], by transcribing it into nonlinear program (NLP) by direct multiple shooting method. The NLP is then solved usinf interior point optimizer (Ipopt) algorithm. The parameters used in the NMPC are $T_p = 25$ s, $\mu_{i_{lb}} = 0$, $\mu_{i_{ub}} = 0.3$, $x_{i_{lb}} = 0.05$ and $x_{i_{ub}} = 0.95$.

The result in figure 4 shows the Pareto front of the two competing sub-objectives–balancing speed and power losses. The balancing speed is characterized by balancing time t_b, which is defined as the time taken by $|\tilde{\hat{x}}|$ to reach 0.02. Whereas, average power loss $\bar{P}_L$ over t_b represents power losses. The result in figure 4 is obtained by simulating 9 different combinations of Q and R (NMPC gains, cf. (13)), in which Q varies from $6 - 700$ and $R = 1$. It can be seen from the figure that for achieving higher balancing speeds, $\bar{P}_L$ also increases.

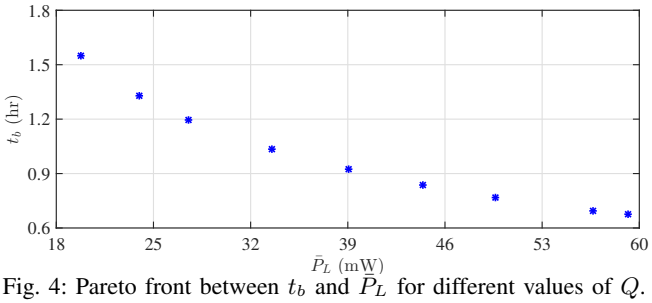

Fig. 4: Pareto front between t_b and $\bar{P}_L$ for different values of Q.

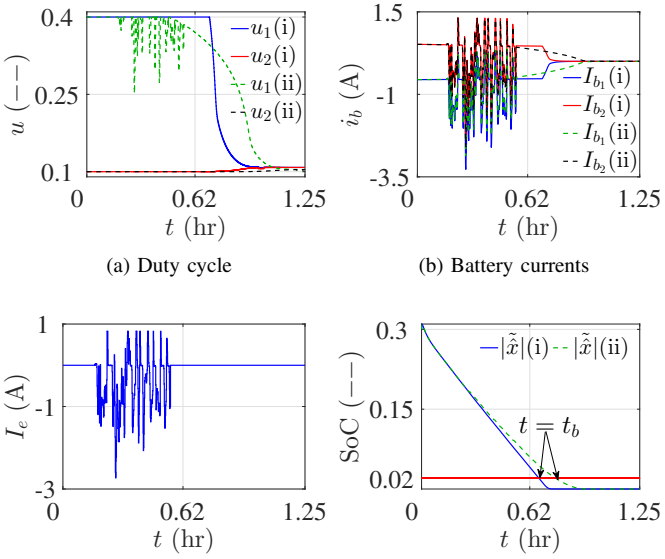

(a) Duty cycle (b) Battery currents

(c) UDDS current profile (d) SoC difference

Fig. 5: Performance comparison of NMPC with different cost function weights.

The performance of NMPC controller with two different choices of the cost functions is compared in figure 5. In case (i) ($Q = 700$, $R = 1$) power losses are almost ignored, whereas, in case (ii) ($Q = 50$, $R = 1$), P_L is relatively given more weight. As $\hat{x}_1 > \hat{x}_2$, therefore, for both cases only Q_1 is on. The controller balances the SoC levels with $t_b = 2425$ s and $\bar{P}_L = 59.17$ mW for case (i), and $t_b = 2770$ s and $\bar{P}_L = 49.62$ mW for case (ii). As the control is relatively expensive in case (ii), therefore, the balancing time is increased by 14.2% and the power losses are decreased by 16.1% as compared to case (i). Moreover, the fluctuations in I_e are also reflected in the duty cycle of case (ii), however, this is not an issue because i) there is no effect on $\hat{x}$ (figure 5d), and ii) the power converters are normally operated at very high frequency.

The results in figure 6 show the performance of SDKF for case (i) discussed previously. The initial values for the states of SDKF are $\vec{\hat{x}}(0) = [0.4\ 0.1]^T$, while the model is initialized with $\vec{x}(0) = [0.5\ 0.2]^T$. The tuning parameters of SDKF are selected as $P_0 = I_{2\times2}$, $\mathcal{Q} = diag(10^{-3}, 10^{-3})$ and $\mathcal{R} = diag(0.25, 0.25)$. The results show that SDKF filters out the noise in $\vec{v}_t$ (figure 6b) and gives a good state estimation (figure 6a). When estimated states converge to their true values, the estimation error does not exceed $|0.8|\%$ for both states.

The results in figure 7 are obtained with NMPC controller having $Q = 700$ and $R = 1$, with three different cases: i) Case (a) ignores all the static and dynamic parameters of the ACBN, which include R_{ch}, R_{dis}, V_F, and the time constants defined in section II; ii) in Case (b) real parameters are used, however, parametric uncertainties, and sensor noises are ignored; and iii) Case (c) has same simulation parameters as Case (i) in figure 5. Due to smaller values of η_i in the ACBN for Case (c),

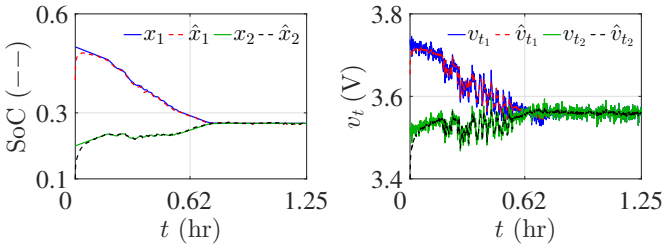

(a) True and estimated SoCs. (b) Measured and estimated voltages.

Fig. 6: Performance of SDKF.

the rate of change of SOC is higher (cf. (8)), which results in smaller t_b, larger currents and $\bar{P}_L$ as compared to Case (b). In case of ideal parameters (Case (a)), the balancing speed is the fastest with zero energy losses. For Case (a), the deviation in t_b from Case (b) and Case (c) is 78.6% and 74%, respectively. This result shows that the controller does not have an absolute control over t_b and $\bar{P}_L$. Moreover, it's essential to include static and dynamic components in the modelling of ACBN for accurate estimation of performance metrics, e.g., t_b and $\bar{P}_L$.

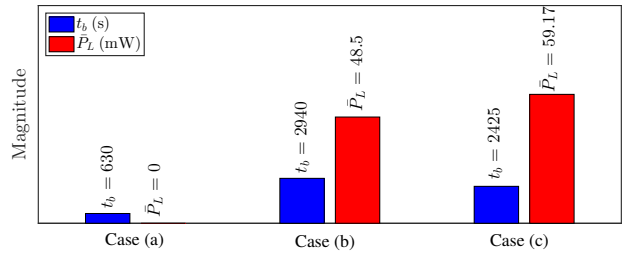

Fig. 7: t_b and $\bar{P}_L$ for different ACBN parameters with same NMPC.

VI. Conclusions

The paper presents a bi-directional SoC equalization based NMPC of an ACBN of any two adjacent cells connected in series. A detailed mathematical model that takes into account the effect of static and dynamic parameters on mean balancing currents and power losses is developed. The robust control scheme successfully meets the balancing criterion, despite the modeling uncertainties and a realistic UDDS current profile. Using Lyapunov theory, the stability of closed-loop system has also been proved. The Pareto front analysis confirms that the conflicting costs of achieving higher balancing speed and reducing energy loss can not be satisfied simultaneously, therefore, a trade-off, depending upon the application is to be made. Furthermore, the simulation results show that i) instead of energy losses, NMPC should give more weightage to SoC balancing to compensate for fluctuations in external currents; ii) the controller, at its best can only balance the SoC levels of cells, and it does not have a complete control over t_b and $\bar{P}_L$, which are also dependent on the static and dynamic parameters of the ACBN; and iii) there is a deviation in t_b if static and dynamic parameters of the ACBN are ignored.

Due to the modular nature of the proposed cell-to-cell balancing approach, it can be easily extended for a string of n series connected cells.

References

[1] F. S. J. Hoekstra, H. J. Bergveld, and M. C. F. Donkers, "Optimal control of active cell balancing: Extending the range and useful lifetime of a battery pack," *IEEE Transactions on Control Systems Technology*, vol. 30, no. 6, pp. 2759–2766, 2022.

[2] A. Pozzi, M. Zambelli, A. Ferrara, and D. M. Raimondo, "Balancing-aware charging strategy for series-connected lithium-ion cells: A nonlinear model predictive control approach," *IEEE Transactions on Control Systems Technology*, vol. 28, no. 5, pp. 1862–1877, 2020.

[3] S. B. Javed, A. A. Uppal, M. R. Azam, K. Shehzad, and Q. Ahmed, "Model-based quantitative analysis of a capacitive cell balancing technique using soc estimator," in *2022 IEEE Conference on Control Technology and Applications (CCTA)*, pp. 670–675, 2022.

[4] J. Chen, A. Behal, and C. Li, "Active cell balancing by model predictive control for real time range extension," in *2021 60th IEEE Conference on Decision and Control (CDC)*, pp. 271–276, 2021.

[5] J. Liu, Y. Chen, and H. K. Fathy, "Nonlinear model-predictive optimal control of an active cell-to-cell lithium-ion battery pack balancing circuit," *IFAC-PapersOnLine*, vol. 50, no. 1, pp. 14483–14488, 2017. 20th IFAC World Congress.

[6] C. N. Van and T. N. Vinh, "Optimal Cell Equalizing Control Based on State of Charge Feedback for Lithium-ion Battery Pack," *International Journal of Control, Automation and Systems*, vol. 21, May 2023.

[7] C. N. Van, "Optimal Control of Active Cell Balancing for Lithium-Ion Battery Pack With Constraints on Cells' Current and Temperature," *Journal of Electrochemical Energy Conversion and Storage*, vol. 20, p. 011009, 05 2022.

[8] F. Hoekstra, H. Bergveld, and M. Donkers, "Range maximisation of electric vehicles through active cell balancing using reachability analysis," in *2019 American Control Conference (ACC)*, pp. 1567–1572, 2019.

[9] F. Hoekstra, L. W. Ribelles, H. Bergveld, and M. Donkers, "Real-time range maximisation of electric vehicles through active cell balancing using model-predictive control," in *2020 American Control Conference (ACC)*, pp. 2219–2224, 2020.

[10] S. M. Salamati, S. A. Salamati, M. Mahoor, and F. R. Salmasi, "Leveraging adaptive model predictive controller for active cell balancing in li-ion battery," in *2017 North American Power Symposium (NAPS)*, pp. 1–6, 2017.

[11] Q. Ouyang, J. Chen, C. Xu, and H. Su, "Cell balancing control for serially connected lithium-ion batteries," in *2016 American Control Conference (ACC)*, pp. 3095–3100, 2016.

[12] J. V. Barreras, C. Pinto, R. de Castro, E. Schaltz, S. J. Andreasen, and R. E. Araujo, "Multi-objective control of balancing systems for li-ion battery packs: A paradigm shift?," in *2014 IEEE Vehicle Power and Propulsion Conference (VPPC)*, pp. 1–7, 2014.

[13] V. Azimi, A. Allam, and S. Onori, "Extending life of lithium-ion battery systems by embracing heterogeneities via an optimal control-based active balancing strategy," *IEEE Transactions on Control Systems Technology*, vol. 31, no. 3, pp. 1235–1249, 2023.

[14] M. C. Teixeira and S. H. Zak, "Stabilizing controller design for uncertain nonlinear systems using fuzzy models," *IEEE Transactions on fuzzy systems*, vol. 7, no. 2, pp. 133–142, 1999.

[15] N. Campagna, V. Castiglia, R. Miceli, R. A. Mastromauro, C. Spataro, M. Trapanese, and F. Viola, "Battery models for battery powered applications: A comparative study," *Energies*, vol. 13, no. 16, 2020.

[16] S. J. Moura, F. B. Argomedo, R. Klein, A. Mirtabatabaei, and M. Krstic, "Battery state estimation for a single particle model with electrolyte dynamics," *IEEE Transactions on Control Systems Technology*, vol. 25, no. 2, pp. 453–468, 2017.

[17] J. Andersson, *A General-Purpose Software Framework for Dynamic Optimization*. PhD thesis, Arenberg Doctoral School, KU Leuven, Department of Electrical Engineering (ESAT/SCD) and Optimization in Engineering Center, Kasteelpark Arenberg 10, 3001-Heverlee, Belgium, October 2013.